





Cite this: *Biomater. Sci.*, 2020, **8**, 438

## Cell loaded 3D bioprinted GelMA hydrogels for corneal stroma engineering†

Cemile Kilic Bektas <sup>a,b,c</sup> and Vasif Hasirci <sup>\*a,b,c,d</sup>

Tissue engineering aims to replace missing or damaged tissues and restore their functions. Three-dimensional (3D) printing has been gaining more attention because it enables the researchers to design and produce cell loaded constructs with predetermined shapes, sizes, and interior architecture. In the present study, a 3D bioprinted corneal stroma equivalent was designed to substitute for the native tissue. Reproducible outer and inner organization of the stroma was obtained by optimizing printing conditions such as the nozzle speed in the *x–y* direction and the spindle speed. 3D printed GelMA hydrogels were highly stable in PBS during three weeks of incubation (8% weight loss). Live–Dead cell viability assay showed 98% cell viability on day 21 indicating that printing conditions were suitable for keratocyte printing. Mechanical properties of the cell loaded 3D printed hydrogels increased 2-fold during this incubation period and approached those of the native cornea (ca. 20 kPa vs. 27 kPa, respectively). Expression of collagens types I and V, and proteoglycan (decorin) in keratocytes indicates maintenance of the phenotype in the hydrogels. Transparency of cell-loaded and cell-free hydrogels was over 80% (at 700 nm) during the three week culture period and comparable to that of the native cornea (85%) at the same wavelength. Thus, GelMA hydrogels bioprinted with keratocytes mimic the biological and physical properties of the corneal stroma with their excellent transparency, adequate mechanical strength, and high cell viability.

Received 5th August 2019,  
Accepted 4th November 2019

DOI: 10.1039/c9bm01236b

rs.c.li/biomaterials-science

### 1. Introduction

The cornea, the outermost and transparent layer of the eye, is about 11–12 mm in diameter and 520  $\mu\text{m}$  in thickness.<sup>1</sup> It is the principal optical element of the eye which refracts about 65–75% of the incoming light. It also acts as a barrier against UV radiation and external and physical objects.<sup>2</sup> The stroma is the thickest part of the cornea and constitutes 90% of the thickness. Collagen type I fibers are the main components of this layer and are organized parallel to each other in one layer and at nearly right angles to the fibers in adjacent layers, much like the fibers in plywood.<sup>3</sup> This organization is critical for both the mechanical strength and the transparency of the cornea.<sup>4</sup> The stroma is populated by sparsely distributed mesenchymal fibroblasts, keratocytes, which preserve the composition and the integrity of the stroma through continuous

production of collagen, proteoglycan, and matrix metalloproteinases.<sup>5</sup>

Corneal blindness caused by injuries or diseases affects the quality of life of millions of people. It is the third major cause of blindness after cataracts and glaucoma. Currently, transplantation is the major and long-term treatment; however, due to shortage of healthy corneas, only 1 in 70 patients is successful in getting one.<sup>6</sup> Keratoprotheses (KPro) are partly synthetic artificial corneas for full thickness replacements. Boston KPro and Osteo-odonto KPro are the two commonly used products on the market.<sup>7</sup> However, degradation of lamina, chronic inflammation, complex design, long surgical procedures, and calcification are some of their reported drawbacks.<sup>8</sup> These imply that alternative, efficient approaches are needed to meet the demand and overcome the limitations of the current treatment methods.

Tissue engineering is a viable alternative to the abovementioned treatments. The complex organization, high transparency and mechanical property requirements make engineering of the corneal stroma a great challenge. To date, a number of scaffolds have been developed for corneal tissue engineering by either mimicking only one layer (epithelium, stroma, or endothelium), two layers (hemi-cornea; epithelium and stroma), or all layers of the cornea.<sup>9–12</sup> These constructs were reported to be produced in various forms like foams, fibers, films, and decellularized cornea tissue.<sup>9,11,13–16</sup> Scaffolds were constructed either using natural materials like silk, gelatin,

<sup>a</sup>Department of Biological Sciences, Middle East Technical University (METU), Ankara, Turkey

<sup>b</sup>Department of Biotechnology, METU, Ankara, Turkey

<sup>c</sup>BIOMATEN, METU Center of Excellence in Biomaterials and Tissue Engineering, Ankara, Turkey

<sup>d</sup>Acibadem Mehmet Ali Aydınlar University, Faculty of Engineering, Department of Medical Engineering, İstanbul, Turkey.

E-mail: vasif.hasirci@acibadem.edu.tr

† Electronic supplementary information (ESI) available. See DOI: 10.1039/c9bm01236b

collagen, and chitosan, or synthetic materials like polyglycolic acid (PGA) and poly(lactic acid-co-glycolic acid) (PLGA).<sup>10,17–21</sup> Insufficient cellular population of the scaffolds, lack of micro-level organization of the corneal stroma, and low light transfer were reported in these studies. Although some of the replacements closely mimicked the physical/chemical organization of the stroma, only a few could manage to reach Phase I of clinical trials.<sup>22</sup> Today there is still no engineered corneal tissue available for routine clinical use.

Gelatin is one of the most widely used natural materials because it is inexpensive, is available from a range of different sources, does not induce any antigenic response, and is suitable for attachment by cells due to its natural cell binding motifs like arginine-glycine-aspartic acid (RGD).<sup>23</sup> Hydrogels composed of gelatin are highly attractive and widely studied in corneal tissue engineering.<sup>19,24</sup> Hydrogels, hydrophilic polymeric networks, are appealing for corneal tissue engineering applications due to their similarity to the natural extracellular matrices, biocompatibility and structural integrity.<sup>25</sup> Researchers have employed a variety of chemicals for the crosslinking of the gelatin like glutaraldehyde, carbodiimide, and NHS.<sup>26,27</sup> However, these approaches have several disadvantages like inability to load cells during gel formation, long processing time, and the use of toxic or bioactive chemicals in crosslinking. Gel formation through photocrosslinking using UV or visible light, therefore, is a popular hydrogel forming technique due to the fast and controllable polymerization and the ability to load cells and other biological molecules into the hydrogel during crosslinking. Gelatin can be conveniently modified by methacrylation and form photocrosslinkable methacrylated gelatin (GelMA). Very short UV exposure (as short as 5 s) and the absence of organic molecules make loading of cells possible during crosslinking.<sup>16,28</sup> GelMA has been used in many tissue engineering applications including meniscus,<sup>29</sup> skin,<sup>30</sup> and bone.<sup>31</sup> Its suitability for corneal wound healing when used together with thiolated gelatin has also been reported.<sup>32</sup> Our group has reported for the first time the use of GelMA hydrogels in corneal stroma engineering.<sup>16</sup> The hydrogels were highly promising in terms of stability, biocompatibility, and transparency. However, they lacked the internal organization of a typical corneal stroma that is crucial for producing a satisfactory corneal stroma. In this study, we improved our product by introducing organization of the keratocytes within the hydrogel that highly mimics the organization in the native structure of the corneal stroma by employing 3D bioprinting. Thus, we achieved organized placement of the keratocytes within the hydrogels to form a construct that more closely mimics the natural tissue.

3D printing is commonly used to build complex structures, including scaffolds, by layer-by-layer deposition of biomaterials by using computer aided design (CAD) data sets.<sup>25,33</sup> 3D bioprinted corneal tissue equivalents have significant potential because of their transparency, high water content and the elasticity requirements of the tissue. These requirements of the tissue are provided by the hydrogels and complex organization of the tissue is mimicked by 3D bioprinting.

3D printing of corneal stroma constructs is very new and a few strategies have been reported by a small number of researchers.<sup>34,35</sup> However, either the inability of the proposed model to mimic the natural organization of the corneal stroma or the high complexity of the system has limited the widespread use of this technique.

In this study, a highly transparent GelMA hydrogel was produced, preparation conditions were optimized, and hydrogels loaded with stromal keratocytes were printed using a simple pneumatic extrusion based bioprinter. The model consisted of parallel fibers within a layer, and adjacent layers at 90° to each other as in the native structure of the stroma. The organization of the stroma was mimicked for the first time by 3D bioprinting of GelMA hydrogels. High cell viability, transparency and adequate mechanical strength obtained with these hydrogels make the construct a strong alternative to the allografts, which are already in short supply.

## 2. Materials and methods

### 2.1 Methacrylated gelatin synthesis

Methacrylated gelatin (GelMA) was synthesized from the reaction of methacrylic anhydride (MA) (Sigma Aldrich, USA) and type A porcine skin gelatin (70–100 bloom, Sigma Aldrich, USA) as described previously.<sup>16</sup> Briefly, 10% (w/v) gelatin solution was prepared in phosphate buffered saline (PBS, pH 7.4, 10 mM) at 60 °C. MA was added to the solution at 50 °C slowly to yield a 20% (v/v) final concentration. After 1 h, the reaction was stopped with warm PBS at 40 °C. Excess methacrylic acid and salts were removed by dialysis (SnakeSkin CO 10 000, Hyclone, USA) against distilled water at 40 °C. The resulting solution was freeze dried (Labconco Freezone 6, USA) and stored at +4 °C until further use.

### 2.2 <sup>1</sup>H nucleic magnetic resonance (<sup>1</sup>H-NMR) of GelMA

Lyophilized GelMA and gelatin were dissolved in D<sub>2</sub>O (30 mg mL<sup>-1</sup>) at 40 °C. <sup>1</sup>H NMR spectra were obtained using a Bruker DPX 400 spectrometer (Germany) at a <sup>1</sup>H resonance frequency of 400 MHz. The degree of methacrylation was 70% as reported earlier.<sup>16</sup>

### 2.3 Preparation of GelMA hydrogel slabs

Hydrogel slabs were prepared on polydimethylsiloxane (PDMS) (Slygard 184, Dow Corning, USA) templates. PDMS templates were prepared by mixing a PDMS prepolymer and catalyst, pouring into glass Petri dishes and curing at 70 °C for 3 h. The resultant PDMS film was peeled off and small discs with different dimensions were prepared ( $h = 0.5$  mm/ $r = 3.5$  mm and  $h = 8$  mm/ $r = 5$  mm). 15% GelMA solution (GelMA15) (w/v, in PBS) was prepared in the presence of 0.5% Irgacure 2959 photoinitiator (2-(hydroxyl)-4-(2-hydroxyethoxy)-2-methylpropiophenone, Sigma Aldrich, USA) (w/v). The solution was poured into the PDMS templates, incubated for 15 min at 4 °C, and crosslinked for 5 s with OmniCure (S1500, Lumen

Dynamics, Canada) ( $15 \text{ mW cm}^{-2}$ , at  $365 \text{ nm}$ ) at a distance of  $3 \text{ cm}$ . The hydrogels were labeled as GelMA15-Slab.

## 2.4 Preparation of 3D printed GelMA hydrogels

GelMA15 solution was prepared as mentioned above and loaded into a  $3 \text{ mL}$  Luer lock syringe compatible with a Bioscaffolder® (SYS-ENG, Salzgitter-Bad, Germany) 3D Printer low temperature dispense head, and incubated at  $4 \text{ }^\circ\text{C}$  for  $15 \text{ min}$ . GelMA was printed at a movement speed of the nozzle in the  $x$ - $y$  direction (Fxy) of  $100$ ,  $200$ , or  $300 \text{ mm min}^{-1}$ , a spindle speed (R/S) of  $0.01$ ,  $0.02$ , or  $0.03$  dots per mm, and from a nozzle with a diameter of  $0.26 \text{ mm}$  ( $25 \text{ ga} \times \frac{1}{2}$  Luer stubs, Instech, USA). The layer thickness and the distance between two strands were set as  $0.14 \text{ mm}$  and  $1 \text{ mm}$ , respectively.

After observation under a stereomicroscope, the following parameters were chosen for further studies: (1) Fxy  $200$  and R/S  $0.01$  (GelMA15-001), (2) Fxy  $200$  and R/S  $0.2$  (GelMA15-002), and (3) Fxy  $300$  and R/S  $0.03$  (GelMA15-003). Rectangular prism GelMA hydrogels ( $14 \times 14 \times 2 \text{ mm}^3$ ) were prepared for mechanical tests, and  $14 \times 14 \times 0.5 \text{ mm}^3$  hydrogels were prepared for other studies (Table 1). Constructs were plotted according to a model prepared using Sketchup (Google Inc., USA) and loaded to the CAM (Computer Aided Manufacturing) software (Prim-CAM, Einsiedeln, Switzerland) of the Bioscaffolder®. Two dimensional (2D) layers were deposited perpendicular to each other at every layer. Models were cross-linked and stored as mentioned above.

## 2.5 Characterization of the hydrogels

**2.5.1 Stereomicroscopy.** 3D printed hydrogels were examined with a Nikon SMZ1500 stereomicroscope (USA) to study the pattern. Hydrogels were stained with Coomassie blue (Sigma Aldrich, USA) ( $0.1\% \text{ w/v}$  in PBS) to ease the observation.

**2.5.2 Scanning electron microscopy.** Hydrogels were lyophilized, coated with Au-Pd under vacuum and examined with a SEM (SEC, Mini-SEM, South Korea) at  $5$ – $20 \text{ kV}$ .

**2.5.3 Equilibrium water content (EWC) of gelMA hydrogels.** Hydrogels were incubated in PBS containing  $0.5 \text{ mg mL}^{-1}$  sodium azide at  $37 \text{ }^\circ\text{C}$ . After  $24 \text{ h}$  of incubation in a shaking incubator, excess liquid on the hydrogels was removed gently with filter paper and wet weights ( $W_w$ ) were recorded. Hydrogels were then rinsed with distilled water, lyophilized

and weighed ( $W_d$ ). The equilibrium water content (%) was calculated from the following equation:

$$\text{EWC (\%)} = \frac{W_w - W_d}{W_w} \times 100 \quad (1)$$

**2.5.4 In situ degradation in PBS.** Initial weights ( $W_0$ ) of the hydrogels were determined after lyophilization ( $n = 3$ ). Samples were then incubated in PBS (pH  $7.4$ ,  $10 \text{ mM}$ ) at  $37 \text{ }^\circ\text{C}$  in a shaking incubator for three weeks. At predetermined time points (days  $1$ ,  $7$ ,  $14$ , and  $21$ ) samples were rinsed with distilled water, freeze dried and weighed ( $W_d$ ). The remaining weight (%) was determined according to the following equation:

$$\text{Remaining weight (\%)} = \frac{W_d}{W_0} \times 100 \quad (2)$$

## 2.6 In vitro studies

**2.6.1 Preparation of cell loaded hydrogel slabs.** Human corneal keratocytes (HKs) were isolated and kindly provided by Prof. Odile D'amour (Banque de Cornées des Hospices Civils de Lyon, Lyon, France). Passage  $5$ – $15$  cells were stored frozen in their medium supplemented with  $15\%$  dimethyl sulfoxide (DMSO, AppliChem, USA) in liquid nitrogen. To culture HKs, cells were thawed and centrifuged, and the cell pellet was suspended in HK medium (growth medium contains Dulbecco's Modified Eagle's Medium–Ham's nutrient mixture F12 (DMEM–HAM's F12,  $1:1$ , Thermo Fisher Scientific, USA), newborn calf serum (Thermo Fisher Scientific, USA) ( $10\%$ ), amphotericin B (Sigma Aldrich, USA) ( $1 \mu\text{g mL}^{-1}$ ), penicillin ( $100 \text{ UI mL}^{-1}$ ), and streptomycin (Sigma Aldrich, USA) ( $100 \mu\text{g mL}^{-1}$ ), and Human basic fibroblast growth factor (bFGF, Cell Signaling Technology, Inc., USA) ( $10 \text{ ng mL}^{-1}$ )). Cells were cultured in tissue culture polystyrene (TCPS) flasks in a  $\text{CO}_2$  incubator (SanyoMCO-17 AIC, Japan) at  $37 \text{ }^\circ\text{C}$ . Cells were trypsinized using trypsin-EDTA ( $0.25\%$ , Sigma Aldrich, USA) at confluence and counted with a NucleoCounter (Chemo-Metec, Denmark).  $1 \times 10^6$  cells per mL was taken in a separate centrifuge tube, centrifuged and suspended directly with GelMA solution prepared with growth medium. The gel precursors were exposed to UV as mentioned above (Fig. 1A). The hydrogel was washed several times with growth medium and incubated in the same medium at  $37 \text{ }^\circ\text{C}$  in a  $\text{CO}_2$  incubator. The medium was changed every two days.

**Table 1** 3D bioprinting parameters used after optimization studies

| Spindle Speed (R/S)<br>(dots per min) | Nozzle Speed (Fxy)<br>( $\text{mm min}^{-1}$ ) | Total number of layers   | Abbreviation |
|---------------------------------------|--|--|--------------|
| 0.01                                  | 200  | 15 – mechanical tests<br>5 – <i>in situ</i> and <i>in vitro</i> tests            | GelMA15-001  |
| 0.02                                  | 200  | 10 layers-mechanical tests<br>3 layers- <i>in situ</i> and <i>in vitro</i> tests | GelMA15-002  |
| 0.03                                  | 300  | 10 layers-mechanical tests<br>3 layers- <i>in situ</i> and <i>in vitro</i> tests | GelMA15-003  |

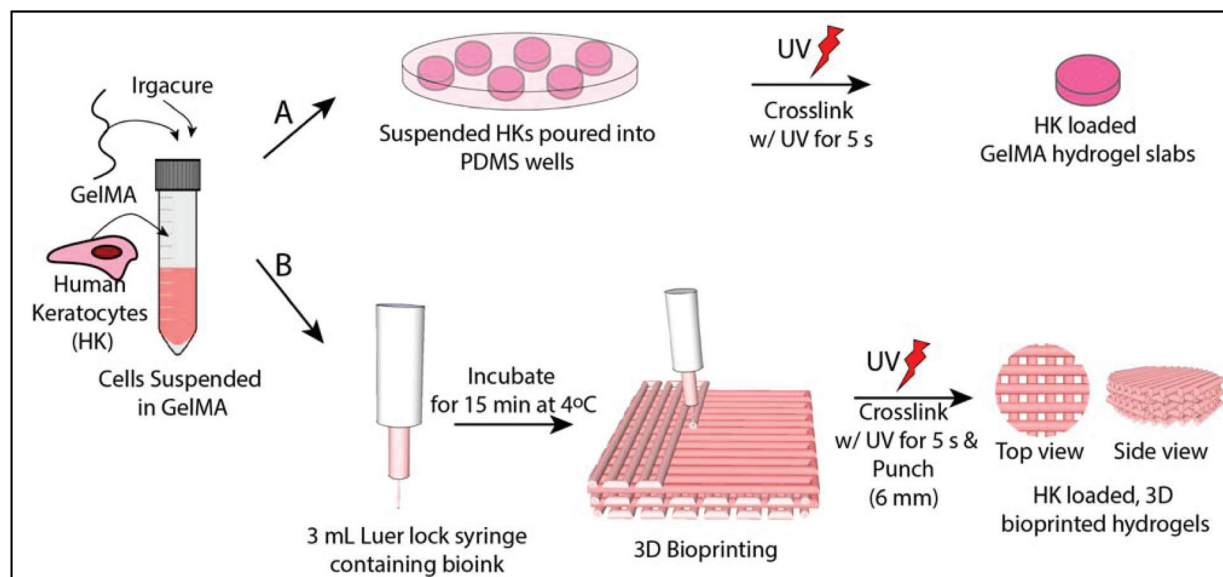


Fig. 1 Schematic representation of preparation of human keratocyte (HK) loaded hydrogels. (A) GelMA slabs, and (B) 3D bioprinted GelMA hydrogels.

**2.6.2 Preparation of 3D bioprinted hydrogels.**  $10^6$  cells per mL of GelMA15 solution (15%, w/v, in HK medium) were prepared. Cell loaded solution (bioink) was introduced to the syringe and incubated for 15 min at 4 °C. Printing of this bioink was carried out as in section 2.4. After crosslinking, 6 mm diameter hydrogels were punched, washed twice with growth medium, and incubated in a CO<sub>2</sub> incubator at 37 °C (Fig. 1B).

### 2.6.3 Microscopical studies

**2.6.3.1 Cell viability.** Cell viability was assessed by using a Live-Dead cell viability/cytotoxicity kit (Thermo Fisher Scientific, USA). Hydrogels were removed from the culture on days 1, 7, 14 and 21, and double stained with Calcein-AM (2 μM in PBS) and ethidium homodimer (EthD)-1 (4 μM) for 30 min at room temperature (RT). Hydrogels were examined under a Zeiss LSM 800 (Germany) Confocal Laser Scanning Microscope (CSLM). Semi-quantitative image analysis ( $n = 3$ ) was performed using ImageJ NIH software to determine the viability of keratocytes (%) in the hydrogels according to the following equation:

$$\text{Viability of cells (\%)} = \frac{\text{Live Cells (Green)}}{\text{Total Cells (Green + Red)}} \times 100 \quad (3)$$

Metabolic activity of the cells was monitored using Alamar Blue® assay (Invitrogen Inc., USA). Samples ( $n = 3$ ) were incubated in Alamar Blue solution (10% v/v in colorless growth medium) for 2 h. Reduction (%) of the dye was calculated according to the manufacturer's instructions using absorbance values obtained at 570 nm and 595 nm.

**2.6.3.2 Immunofluorescence staining.** Hydrogels were removed from the growth medium, HKs were fixed with 4% paraformaldehyde (PFA, Sigma Aldrich, USA) (w/v) for 30 min at RT, and their cell membranes were permeabilized with 1% Triton X-100 (AppliChem, USA) (v/v, in PBS) for 5 min. For

blocking, samples were incubated in 1% bovine serum albumin (BSA, Sigma Aldrich, USA) (w/v, in PBS) at 37 °C for 1 h. Solutions of primary antibodies against collagen type I (1 : 100 v/v), collagen type V (1 : 100 v/v), decorin (4.8 μg mL<sup>-1</sup>), and α-SMA (1 : 100 v/v) (all from Abcam Inc., MA) were prepared in 0.1% BSA (w/v, in PBS). Hydrogels were incubated with these primary antibodies overnight at 4 °C. The next day, samples were washed with PBS twice for 5 min and incubated with secondary antibodies (either anti-rabbit or anti-mouse Alexafluor 488 secondary antibody) (Invitrogen Inc., USA) (1 : 100 v/v in 0.1% BSA in PBS) at 37 °C for 1 h. Hydrogels were then rinsed twice for 5 min and nuclei of the cells were stained with DRAQ5 (Thermo Fisher Scientific, USA) (1 : 1000 v/v in 0.1% BSA in PBS) for 1 h, at RT. Hydrogels were rinsed twice and stored in PBS until examination by CLSM.

**2.6.4 Mechanical properties of cell loaded and cell free hydrogels.** Cell loaded ( $1 \times 10^6$  cells per mL) and cell free hydrogels were prepared and tested mechanically under compression ( $n = 5$ ) by using a 10 N load cell (Univert, Canada) at a displacement rate of 1 mm min<sup>-1</sup> speed at room temperature. Hydrogels were tested on days 1, 7, 14 and 21 and kept in growth medium until testing. Compressive moduli of the scaffolds were calculated from the slope of the very first linear region of the stress strain curve according to the study by Harley *et al.*, (2007).<sup>36</sup> The following equations were used in the calculations:

$$\text{Stress} : \sigma = \frac{F}{A} \quad (4)$$

$$\text{Strain} : \varepsilon = \frac{\Delta l}{l} \quad (5)$$

$$\text{Compressive Modulus} : \frac{\sigma}{\varepsilon} \quad (6)$$

where  $F$ : applied force (N),  $A$ : cross-sectional area ( $\text{mm}^2$ ),  $l$ : initial sample length (mm), and  $\Delta l$ : displacement

**2.6.5 MMP activity of the cell loaded hydrogels.** MMP activity in the supernatant of cell culture media was measured by using a fluorometric MMP assay kit (SensoLyte® 520 Generic, AnaSpec Inc., USA) according to the manufacturer's instructions. Briefly, cell culture media were collected at every media change, centrifuged for 15 min at 1000g, +4 °C, and stored at -80 °C until use. At the end of 21 days of incubation, collected culture media were thawed and incubated in 1 mM 4-aminophenylmercuric acetate (APMA, Component C of the kit that is diluted with Component D) for 3 h at 37 °C to activate the MMPs. Samples were then loaded into 96 well plates (50  $\mu\text{L}$  per well) and MMP substrate solution (50  $\mu\text{L}$  per well) (Component A of the kit that is diluted with Component D) was added and incubated for 1 h, at RT. To stop the reaction, Component E was added (50  $\mu\text{L}$  per well) to the wells and fluorescence intensity was measured at  $E_x$  and  $E_m = 490$  nm and 520 nm, respectively. Assay buffer (Component D)-containing wells served as the substrate control. Relative fluorescence units (RFU) were obtained by subtracting the control substrate reading from all readings. MMP activity in  $\mu\text{M}$  was calculated according to a calibration curve plotted by using the 5-FAM-Pro-Leu-OH standard (Component B) (Fig. S1†). The number of cells in each sample was used to normalize the MMP activity results.

**2.6.6 Transparency of the hydrogels.** Cell loaded ( $1 \times 10^6$  cells per mL) and cell free hydrogels were scanned in the 250–700 nm range by using a Multiscan UV Visible spectrophotometer (Thermo Scientific, USA) on days 1, 7, 14, and 21. Wells containing only growth medium served as the blank. The average value of blanks was deducted from the sample readings and transmittance values were obtained.

## 2.7 Statistical analysis

The GraphPad Prism program (Version 6.01) was used for statistical analysis. Two-way analysis of variance (ANOVA) with Tukey's *post hoc* test or Student's *t* test was used depending on the number of comparisons. Data are given as mean  $\pm$  standard deviation (SD) ( $n = 3$ ) and  $p \leq 0.05$  was reported as statistically significant.

# 3. Results and discussion

## 3.1 Optimization of printing conditions

Models created by the Sketchup program were transferred as .stl files to the 3D printer, Bioscaffolder®. A low temperature dispense head was used and the fiber thickness was controlled with parameters such as the movement speed of the nozzle in the  $x$ - $y$  direction ( $F_{xy}$ ,  $\text{mm min}^{-1}$ ) and spindle speed (R/S, dots per min). The thickness of the fibers decreased as  $F_{xy}$  increased (Fig. 2). On the other hand, the fiber thickness increased as R/S increased. Printing conditions were optimized as presented in Fig. 2A. It was observed that the nozzle speed

has an optimum at 200  $\text{mm min}^{-1}$  when the spindle speed was set at 0.01 or 0.02 dots per min. Under these conditions, the gaps are well defined and the line thicknesses are quite consistent (Fig. 2B). Similarly, the model was properly printed at 300  $\text{mm min}^{-1}$  nozzle speed and 0.03 dots per min spindle speed. These parameters were used in the following studies. Hydrogels which were prepared as slabs (section 2.3) were labeled as GelMA15-Slab. All 3D printed and slab hydrogels were stable after crosslinking. SEM images of the selected hydrogels clearly show the patterns and open pore structure of the scaffolds (Fig. S2†). Hydrogels retained a significant amount of water in their structures (*ca.* 90%), which is important to give cells space to proliferate.

## 3.2 Degradation of hydrogels under *in situ* conditions

The *in situ* stability of the hydrogels was studied by incubating in PBS (pH 7.4, 10 mM, 0.5  $\text{mg mL}^{-1}$  sodium azide) for three weeks. 3D printed and slab hydrogels were very stable and lost only 8% of their initial weights in 21 days (Fig. 3). Degradation rates of all hydrogels were similar and there was no statistically significant difference between them. The high stability of the hydrogels is most probably due to two reasons: (1) a high UV intensity was used in crosslinking, and (2) 3D printed hydrogels were incubated at 4 °C prior to crosslinking for physical gelation. The stability of the hydrogels, therefore, was enhanced due to dual crosslinking mechanisms which are physical (low temperature) and chemical (due to UV exposure). Other researchers reported similar results in terms of enhanced stability and mechanical properties due to physical gelation prior to chemical crosslinking.<sup>37–39</sup> This phenomenon is known as the sol-gel transition which is induced thermally and a physical crosslinking takes place through noncovalent interactions.<sup>40</sup> Most of the natural polymers like cellulose,<sup>41</sup> agarose,<sup>42</sup> and gelatin<sup>43</sup> exhibit sol-gel behavior upon reduced temperature. Researchers suggest that crosslinking after these physical associations results in a more efficient covalent bond formation due to increased proximity of the polymer chains.<sup>38</sup> In this study, physical gelation enhanced the production of the planned pattern and product; otherwise it is impossible to obtain printed architecture in a liquid phase.

## 3.3 *In vitro* studies

**3.3.1 Live-Dead cell viability test of keratocytes in 3D printed hydrogels.** Human keratocyte (HK) loaded hydrogels were double stained with Calcein AM (stains live cells green), and ethidium homodimer (stains dead cells red) in order to study the viability of the cells in the 3D printed hydrogel lines. Fig. 4A shows high viability of cells on day 21 (results of days 1, 7, and 14 are given in Fig. S3†). The depth profile of day 21 shows a homogeneous distribution of cells within the hydrogels throughout the 500  $\mu\text{m}$  thickness of the structure (Fig. 4A). The fraction of live cells in the hydrogels was calculated using the NIH Image J program (Fig. 4B) which indicates that over 95% of the cells were alive in all types of hydrogels for 3 weeks. High viability of HKs indicates that the printing conditions are appropriate for cell viability. Other researchers

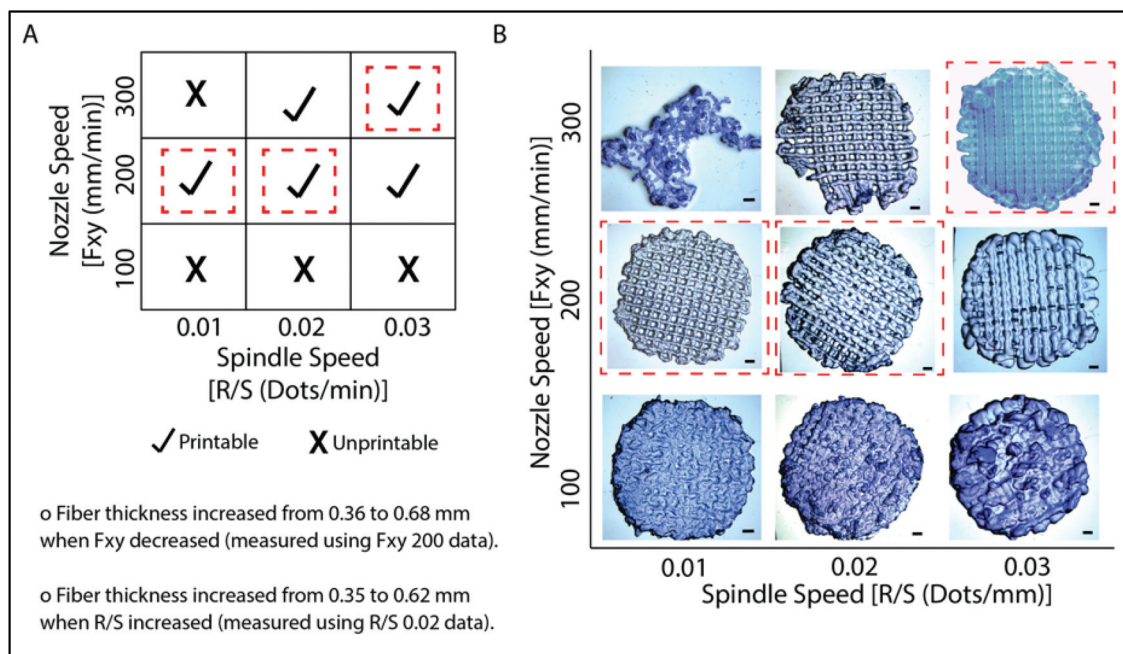


**Fig. 2** Printing conditions and appearance of 3D printed GelMA hydrogels. (A) Print condition optimization of the hydrogels under varying conditions of speed of the nozzle in the  $x$ - $y$  direction (Fxy,  $\text{mm min}^{-1}$ ) and spindle speed (R/S, dots per min). Dotted red lines indicate parameters selected for use in the following studies. (B) Stereomicrographs of the hydrogels. The scale bar is 1 mm.

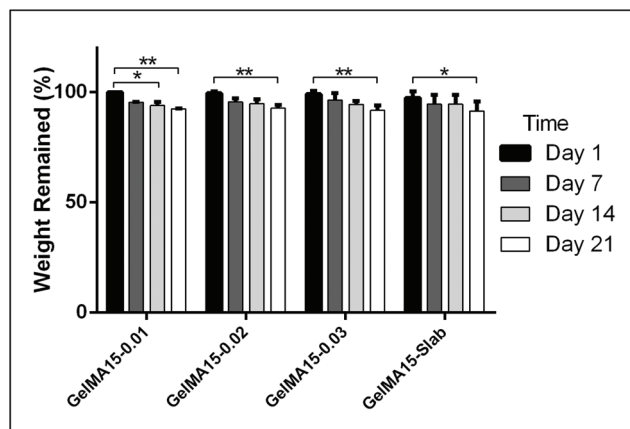


**Fig. 3** *In situ* stability test of 3D printed hydrogels (in PBS, pH 7.4, 10 mM) for 3 weeks. \* $p < 0.05$ , \*\* $p < 0.01$ , and \*\*\* $p < 0.001$ .

reported a wide range of viability results (35%–92%) for cells in GelMA hydrogels.<sup>39,44–46</sup> A number of processing conditions such as GelMA concentration, crosslinking and printing parameters all affect cell viability and the result of our present study is one of the best.

Mesenchyme-derived fibroblasts, keratocytes, are sparsely distributed in the stroma and normally form an interconnected cellular network.<sup>5</sup> However, HKs loaded in 3D printed hydrogels were mostly round in shape, most probably due to a tight network caused by physical crosslinking prior to UV exposure. This might limit the mobility of the cells and

prevent cell interaction and elongation. Studies suggest that cells try to form stable contacts with the surrounding cells through their extensions and if this contact does not occur, they retract them.<sup>47</sup> Cells in the hydrogels, therefore, might not interact with each other due to dense crosslinking and may not elongate. Similar results were reported by other researchers; for example gradually increasing concentration of GelMA hydrogels (from 5% to 30%) led to an increase in crosslink density and rigidity and thus to more round shaped cells.<sup>39</sup> In several studies, researchers attempted to develop new methodologies like pre-crosslinking of the hydrogel solution (GelMA + gelatin or alginate) physically by thermal or ionic interactions to enhance printability of GelMA at low concentrations ( $\leq 5\%$ ).<sup>39,46</sup> Alternatively, the cell density can be increased to obtain more interacting cells. A common seeding density of cells reported as  $2 \times 10^6$  cells per mL by many studies<sup>35,48</sup> can be used to enhance the interactions of the cells with each other. Morphology of the constructs was also shown to affect the behavior of cells. In a recent study, cells grown on curved constructs spread, elongated, produced an aligned extracellular matrix (ECM), and expressed corneal stromal cell markers without the need for any additional cues.<sup>49</sup> The 3D printed construct proposed in our study, therefore, may be further improved by mimicking the curvature of the cornea either by printing on a curved template or crosslinking the printed structure while on a curved template for the construct.

**3.3.2 Cell proliferation in 3D printed hydrogels.** Alamar Blue assay was used to study proliferation of cells in the hydrogels. The results were compared with the number of cells

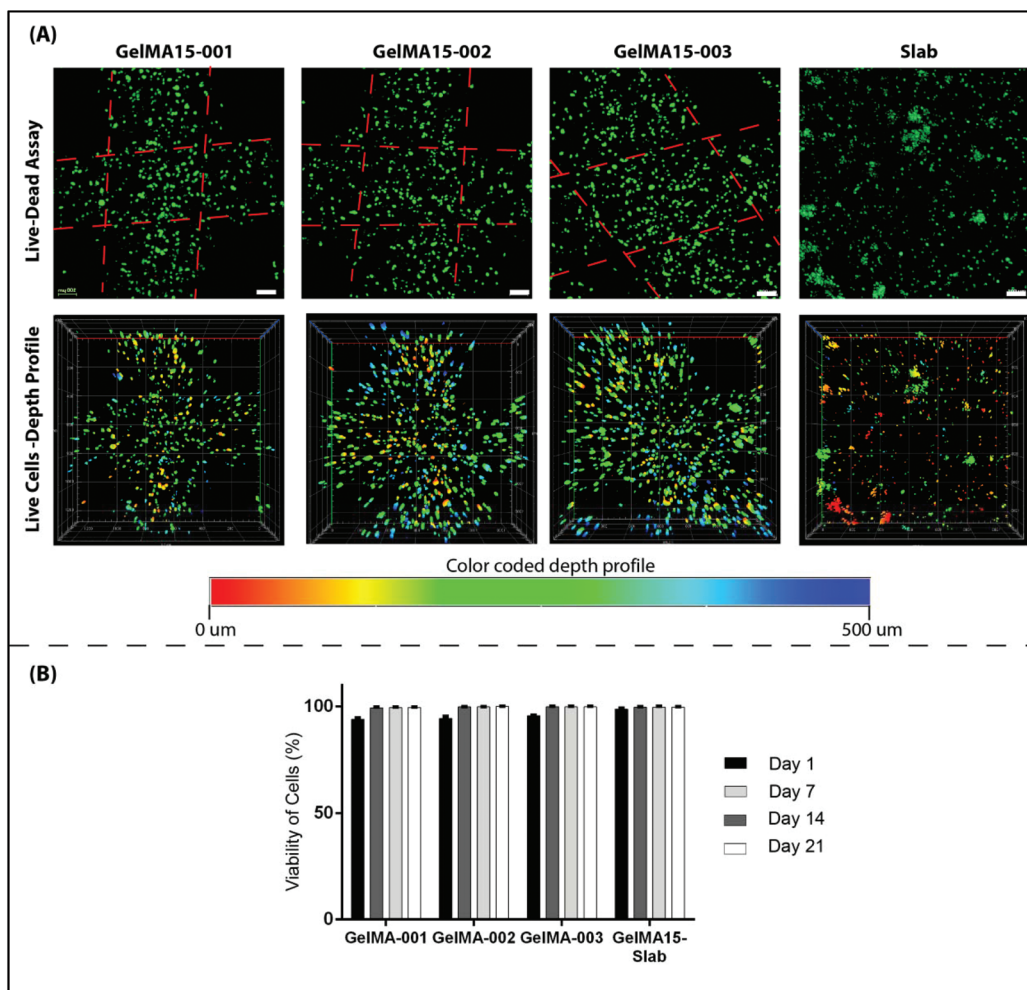


Fig. 4 CLSM images showing results of Live-Dead cell viability assay of 3D printed and slab GelMA hydrogels on day 21. (A) Live-Dead assay with red showing dead (ethidium homodimer-1) and green showing live cells (calcein). Color coded depth profile of the same images showing the distribution of live keratocytes in 3D printed GelMA hydrogels (red: surface and blue: bottom). Scale bars: 100  $\mu\text{m}$ . Dotted red lines indicate line borders. (B) Quantitative analysis carried out using the NIH ImageJ program shows viability of cells (%) over a period of 3 weeks.

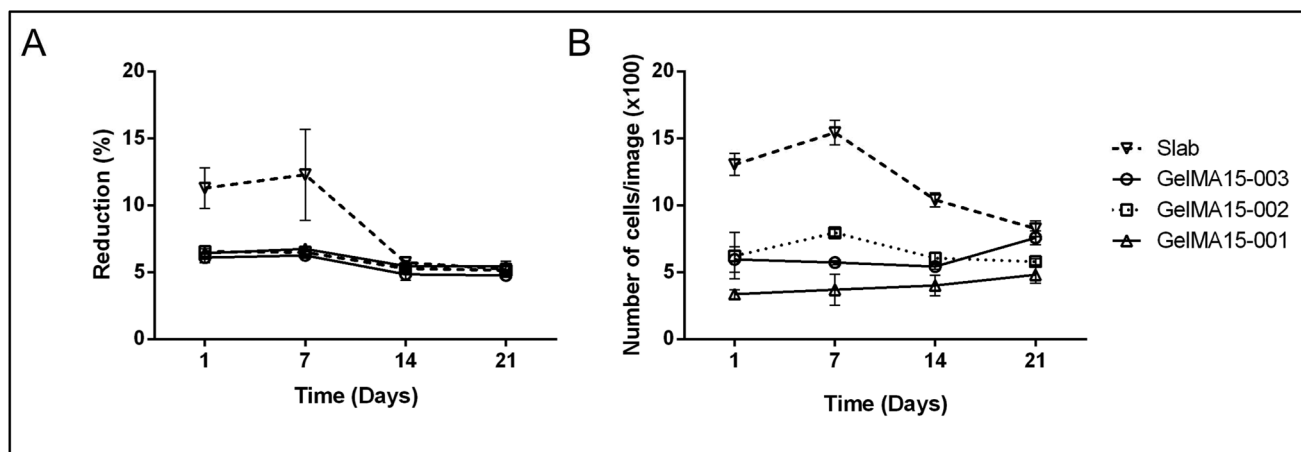


Fig. 5 Proliferation of human keratocytes in 3D Printed and GelMA15-Slab hydrogels over 3 weeks. (A) Alamar Blue assay shows proliferation of cells in the hydrogels as indicated by the reduction % and (B) Live-Dead viability assay images (Fig. 4B and Fig. S3†) were used to count the number of cells per image ( $n = 3$ ) with the NIH Image J program.

determined with the NIH Image J program using the Live-Dead viability assay images obtained by confocal imaging (Images of Fig. 4B and Fig. S3† were used in these determinations) ( $n = 3$ ) (Fig. 5). The number of cells was found to be much lower than that on TCPS (data not shown) because they were entrapped in the hydrogels. The cell number (or activity) in slab gels was higher on days 1 and 7 than those 3D printed hydrogels both in Alamar Blue and Live-Dead tests (Fig. 5). The cell numbers in the 3D printed samples did not change significantly during the incubation period. However, the number of cells in the GelMA15-Slab hydrogels decreased significantly from day 7 to day 14 in both Fig. 5A and B. The reason can be the degradation of the hydrogels which lead to material and cell loss. High crosslinking density is expected due to the physical gelation step prior to UV exposure as discussed above and this might limit the mobility of the cells, nutrient and oxygen transport throughout the hydrogels.

**3.3.3 Mechanical properties of cell loaded hydrogels under compression.** Mechanical properties of cell loaded and cell free (control) 3D printed and slab hydrogels were determined under compression (Fig. 6). Results showed that the compressive modulus of only the cell loaded 3D printed hydrogels increased significantly from day 1 to day 21 and there was no statistically significant difference between other groups (Fig. 6). The compressive modulus of the native human cornea was reported to be between 27 and 41 kPa by several researchers.<sup>50,51</sup> In this study, the compressive modulus of the 3D printed hydrogels was around 10 kPa at the beginning of the test and it increased significantly up to 20 kPa in cell loaded hydrogels. It, therefore, seems that the activity of HKs contributes to the mechanical properties of the constructs through the synthesis of collagens and proteoglycans (see Fig. 7). Earlier studies by our group had also shown that the culture of the corneal keratocyte seeded scaffolds for a month enhances the mechanical properties of the construct significantly.<sup>52,53</sup> We have also shown recently that the chemi-

cal composition of the final hydrogel construct can be modified with introduction of other polymers like poly(2-hydroxyethyl methacrylate) (pHEMA) to enhance mechanical properties.<sup>54</sup> The slight but not significant increase in the compressive modulus of other samples, unseeded controls and slab hydrogels may be attributed to the nonenzymatic glycation through crosslinking of proteins by reducing sugars during incubation in the growth medium.<sup>55,56</sup>

In this study, compressive tests were carried out to give an idea as to where the product stands in terms of mechanical strength compared to native cornea. Besides, compression tests for corneal constructs are a very widely reported and recommended technique in the literature<sup>37,57,58</sup> since the cornea faces significant intraocular pressure in its native environment.

### 3.3.4 Extracellular matrix synthesis by human keratocytes entrapped in the 3D printed hydrogels and hydrogel slabs.

ECM synthesis of the HKs entrapped in 3D printed gels and slab hydrogels was studied on day 21 by staining with HK specific collagens (types I and V) and proteoglycan (decorin), with  $\alpha$ -SMA serving as a control marker.<sup>16,18</sup> Micrographs showed that collagens and decorin were synthesized by only the cells at the edge of the lines (Fig. 7) because very low or no signal was detected in the cores. Similarly, only the HKs close to the surface of the hydrogel slabs synthesized ECM molecules as was observed during CLSM studies. These results suggest that cells at the surface have more growth medium and oxygen in the environment and thus could express ECM molecules, while those inside the hydrogels, though alive, could not (Fig. 4, Live-Dead analysis); apparently, they could not produce the ECM because they were not metabolically active. The high crosslinking density of 3D printed hydrogels due to strong UV intensity and dual crosslinking may have restricted the mobility of the cells, and limited their access to oxygen and growth medium, and there was no ECM expression. HKs in GelMA15-001 and GelMA15-002 hydrogels, however, expressed more collagen and decorin compared to GelMA15-003 hydrogels. This may be because of the smaller surface area of GelMA15-003 hydrogels due to their fibers being thicker than other 3D printed hydrogels. Alpha smooth muscle actin ( $\alpha$ -SMA) expression could not be detected or was significantly lower than other corneal keratocyte specific markers. In intact cornea, HKs are relatively quiescent. Their function is to maintain the levels of collagen and other ECM components and they do not normally express  $\alpha$ -SMA. However, upon injury keratocytes are transformed to myofibroblast-like cells which are characterized by pharmacologic, morphologic and biochemical features similar to those of myofibroblasts.<sup>59</sup> Significantly lower expression of  $\alpha$ -SMA suggests that the keratocytes did not transform into myofibroblast-like cells and preserved their keratocyte features.

The expression of cornea-specific proteins and proteoglycans can be enhanced by increasing the loaded cell density to help cells to communicate with each other. Crosslinking conditions (photoinitiator concentration, UV duration and distance) can be optimized to obtain hydrogels with lower cross-

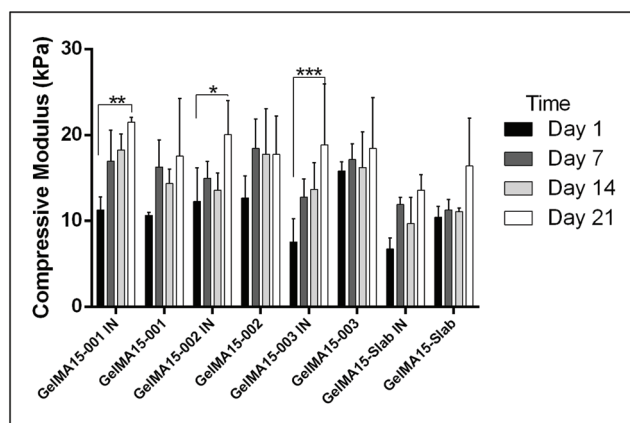


Fig. 6 Compressive moduli change of cell loaded IN 3D printed, unloaded 3D printed, cell loaded GelMA15-Slab and unloaded GelMA15-Slab hydrogels over 3 weeks. IN: with cells. \* $p < 0.05$ , \*\* $p < 0.01$ , and \*\*\* $p < 0.001$ .



linking density to enhance the growth medium and oxygen transport into the hydrogels.

**3.3.5 MMP activity of the keratocytes loaded into 3D printed hydrogels and hydrogel slabs.** MMP activity of the HK loaded in 3D printed and slab hydrogels was studied for 21 days in samples obtained from the culture medium. MMPs

secreted and diffused into the culture medium were determined by using the MMP assay kit. MMP activities of the keratocytes in 3D printed hydrogels gradually increased over time but were significantly lower than those in the slabs, with the exception of day 1 (Fig. 8). This difference can be explained by the cell proliferation profile of the samples. As discussed in

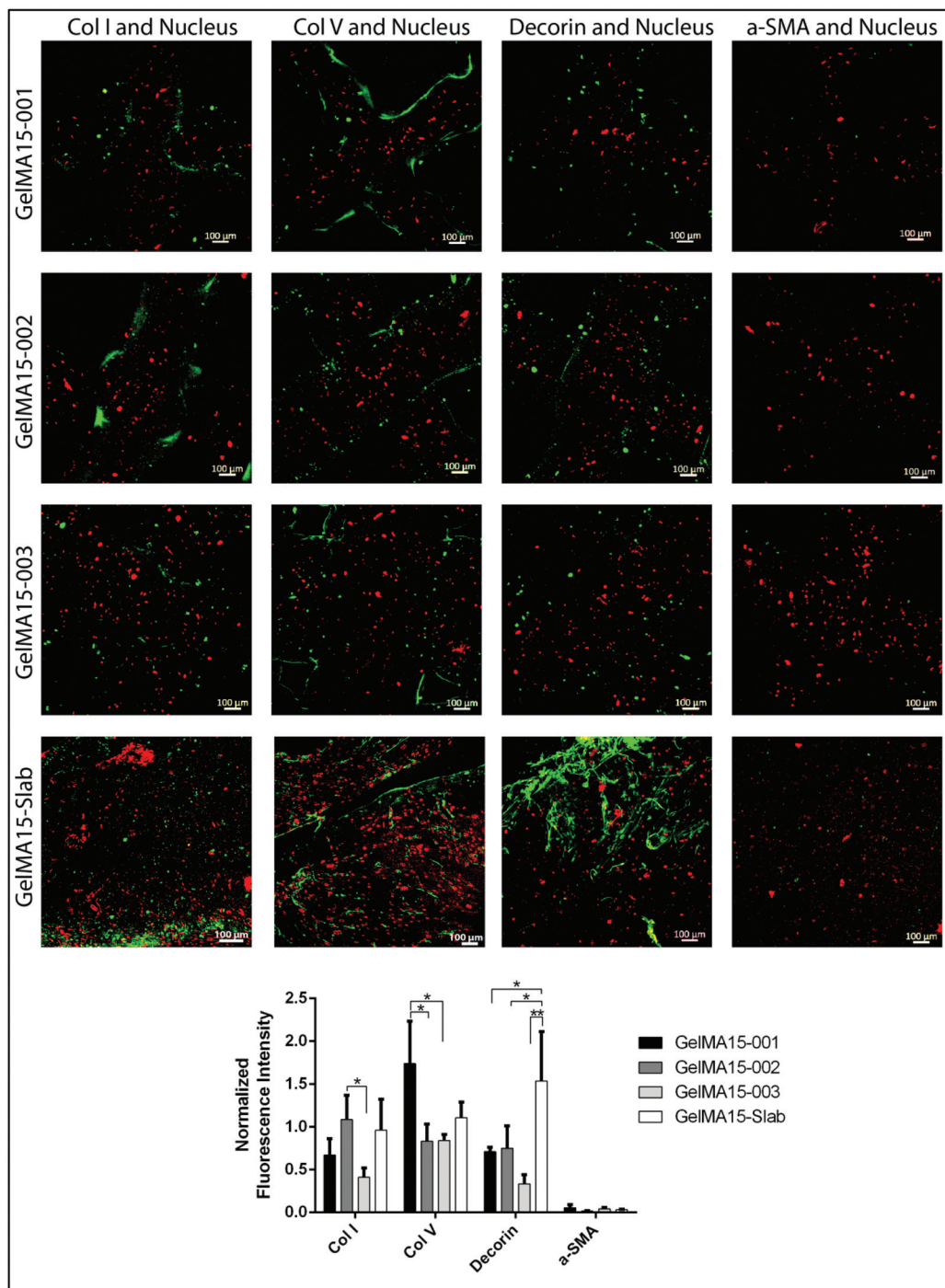


**Fig. 7** Immunocytochemistry results of 3D printed and slab hydrogels. (A) CLSM images on day 21. Draq5 is for nucleus staining (red). Representative collagens (collagen type I and V), proteoglycan (decorin), and myofibroblast marker  $\alpha$ -SMA are shown in green. The scale bar is 100  $\mu$ m. (B) Semi-quantitative fluorescence intensity analysis of CLSM images determined by NIH Image J.  $n = 3$ . \* $p < 0.05$  and \*\* $p < 0.01$ .

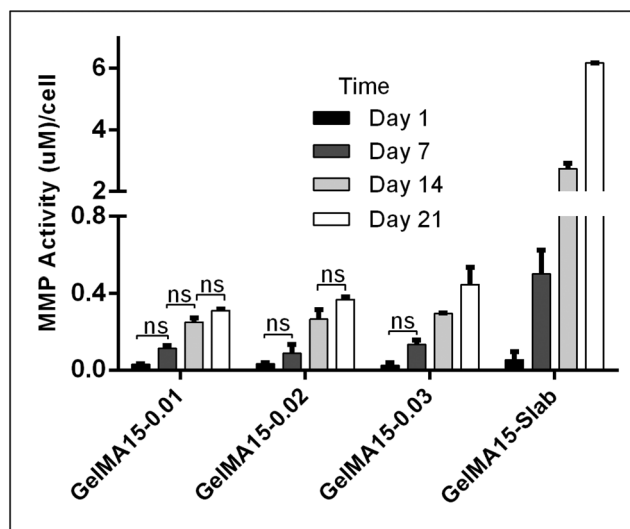


**Fig. 8** MMP activities of the keratocytes in the hydrogels during 21 days of culture. MMP concentrations were normalized by the number of cells calculated from Alamar Blue assay (section 3.3.2). Only non-significant data (ns) are presented on the figure.

section 3.3.2, proliferation of the cells in the 3D printed hydrogels was very low compared to cells in the Slab. MMP activity of the HKs is given as cumulative (day 21 medium also contains days 1, 7, and 14 media) and therefore the effect of the cell number decrease is not seen on the graph. Moreover, the decrease in the cell number can be explained by a continuous increase in MMP activity. MMPs (especially collagenase and gelatinase) are activated in injured corneas for the wound healing mechanism.<sup>60,61</sup> They also degrade the GelMA constructs.<sup>16</sup> Material loss due to collagenase activity, therefore, may also have led to cell loss. As discussed in the previous section (3.3.2), cells in the fibers of the 3D printed hydrogels were most probably not metabolically active due to limited nutrients and oxygen, which explains the low MMP activity. For the regeneration of tissue and removal of the constructs by the mechanisms of the host *in vivo* degradation of the constructs by MMPs is essential. MMPs of the surrounding tissue may also help degradation of the constructs *in vivo*.

**3.3.6 Transparency of cell loaded, 3D printed hydrogels.** Transparency of the cornea is its most important property

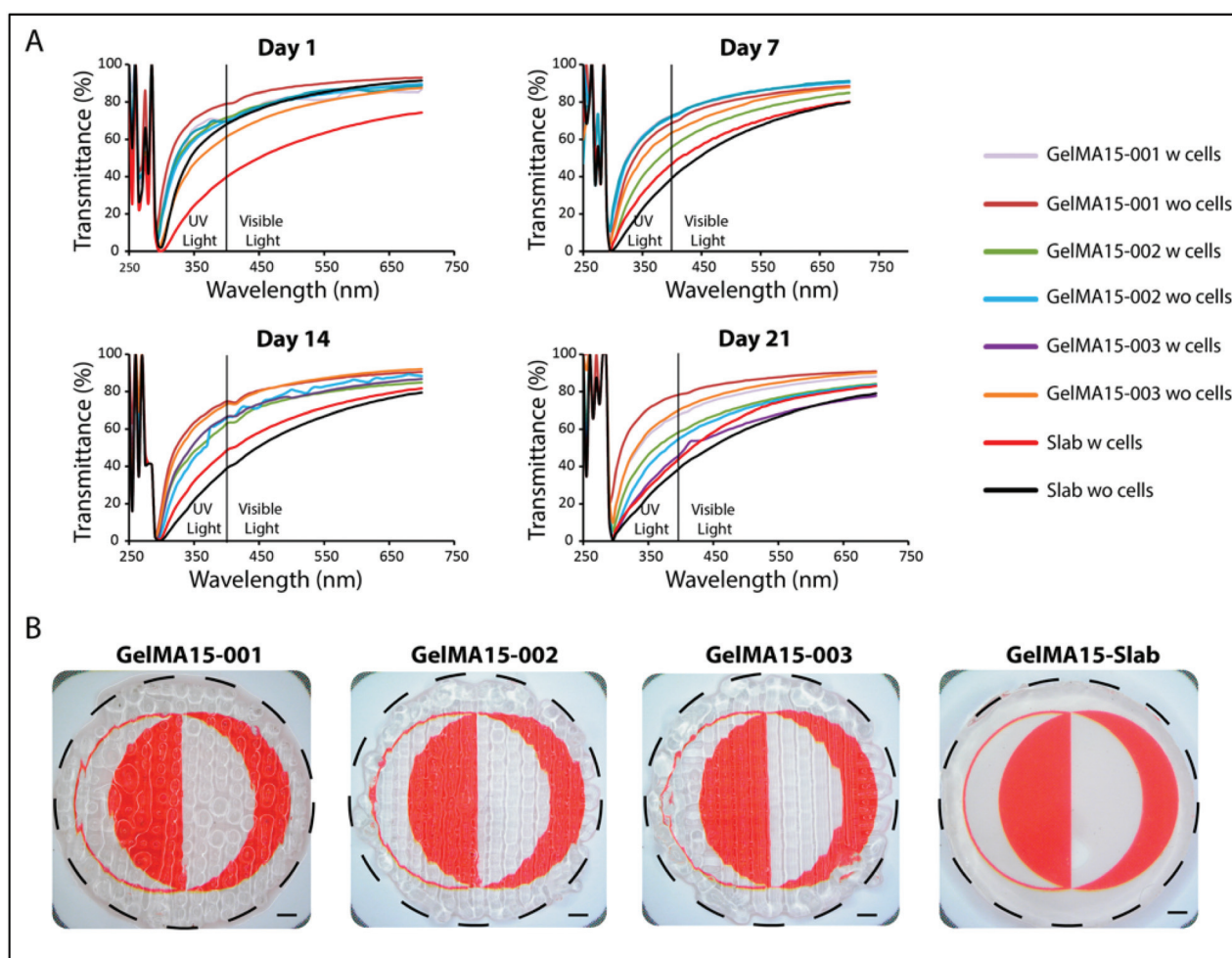


**Fig. 9** Light transmission of the 3D printed hydrogels. (A) Change of transparency of the cell free and keratocyte carrying hydrogels with incubation time. (B) Stereomicrographs showing transparency of cell free hydrogels on day 0 (outlined in black). The scale bar is 1 mm. w: with, wo: without.

because it is where the light is refracted onto the lens and transmitted eventually onto the retina. Transparency of all hydrogels was 80% or higher except for the cell loaded slab hydrogels on day 1; it was about 75% at 700 nm (Fig. 9A and Table S1†). The reason for this lower transparency is most probably because of the higher density of cells in the slab compared to others (section 3.3.2). Light transmittance of these slabs, however, increased during the culture to around 83%.

In the 290–400 nm range, transmittance was lower; this is the UVA and UVB regions and the transparency is comparable to that of the natural cornea (~5% at UVB and 85% at 700 nm for a cornea of an 8 years old).<sup>62</sup> However, transmittance at 300 nm (Table S1†) of slab hydrogels was lower than that of the 3D printed hydrogels (Table S1†). In conclusion, although light was scattered because of the patterns of 3D printed hydrogels, their transparency was still comparable with each other and with native cornea. The clarity of the 3D printed and slab hydrogels is seen in the stereomicrographs (Fig. 9B).

In this study, GelMA hydrogels bioprinted with human corneal keratocytes were shown to mimic the native structure of the corneal stroma with their excellent transparency, adequate mechanical strength and high cell viability. Our recent pilot *in vivo* study on rabbits has also proven the biocompatibility and biodegradability of the GelMA hydrogels<sup>63</sup> which is an important indication of the potential of GelMA hydrogels for use in corneal stroma engineering applications.

## 4. Conclusion

In this study, highly transparent, biocompatible, and stable corneal stroma equivalents were produced by a rapid and effective 3D bioprinting method that mimics the micro-level organization of the stroma. In addition, high cell viability demonstrated the suitability of the printing process and conditions for the production of cell seeded corneal stroma. Synthesis of the specific collagens and proteoglycan by the seeded keratocytes indicated the maintenance of the cell phenotype during printing and under culture conditions. Optimization of the cell density in the hydrogels is necessary to promote the natural interaction and alignment of the cells. *In vivo* performance of the 3D printed hydrogels is also essential to show the compatibility of this biomaterial before clinical studies. These findings show great promise for the application of 3D bioprinting in corneal stroma engineering.

## Conflicts of interest

The authors have declared that there is no conflict of interest.

## Acknowledgements

The authors gratefully acknowledge BIOMATEN and the financial support from METU through BAP-01-08-2013-003 and

BAP08-11-DPT-2011-K120350 projects and TUBITAK for the BIDEB2211-C Scholarship for C. K.

## References

- 1 J. W. Ruberti and J. D. Zieske, *Prog. Retinal Eye Res.*, 2008, **27**, 549–577.
- 2 P. E. Ludwig and K. Sevensma, *Anatomy, Head and Neck, Eye Cornea*, 2019.
- 3 N. J. Fullwood, *Structure*, 2004, **12**, 169–170.
- 4 J. Torbet, M. Malbouyres, N. Builles, V. Justin, M. Roulet, O. Damour, Å. Oldberg, F. Ruggiero and D. J. S. Hulmes, *Biomaterials*, 2007, **28**, 4268–4276.
- 5 J. A. West-Mays and D. J. Dwivedi, *Int. J. Biochem. Cell Biol.*, 2006, **38**, 1625–1631.
- 6 P. Gain, R. Jullienne, Z. He, M. Aldossary, S. Acquart, F. Cognasse and G. Thuret, *JAMA Ophthalmol.*, 2016, **134**(2), 167–173.
- 7 B. Salvador-Culla and E. P. Kolovou, *J. Funct. Biomater.*, 2016, **7**, 13.
- 8 R. Viitala, V. Franklin, D. Green, C. Liu, A. Lloyd and B. Tighe, *Acta Biomater.*, 2009, **5**, 438–452.
- 9 N. E. Vrana, N. Builles, V. Justin, J. Bednarz, G. Pellegrini, B. Ferrari, O. Damour, D. J. S. Hulmes and V. Hasirci, *Invest. Ophthalmol. Visual Sci.*, 2008, **49**, 5325–5331.
- 10 C. Kilic, A. Girotti, J. C. Rodriguez-Cabello and V. Hasirci, *Biomater. Sci.*, 2014, **2**, 318.
- 11 A. Acun and V. Hasirci, *J. Biomater. Sci., Polym. Ed.*, 2014, **25**, 1110–1132.
- 12 S. Wang, C. E. Ghezzi, R. Gomes, R. E. Pollard, J. L. Funderburgh and D. L. Kaplan, *Biomaterials*, 2017, **112**, 1–9.
- 13 M.-I. Huh, K.-P. Lee, J. Kim, S. Yi, B.-U. Park and H. K. Kim, *J. Ophthalmol.*, 2018, **2018**, 1–18.
- 14 L. S. Wray and E. J. Orwin, *Tissue Eng., Part A*, 2009, **15**(7), 1463–1472.
- 15 P. Zorlutuna, A. Tezcaner, I. Kiyat, A. Aydinli and V. Hasirci, *J. Biomed. Mater. Res., Part A*, 2006, **79**, 104–113.
- 16 C. Kilic Bektas and V. Hasirci, *J. Tissue Eng. Regener. Med.*, 2018, **12**, e1899–e1910.
- 17 S. Hong, J. H. Yun, E.-S. Kim, J. S. Kim, H. Tchah and C. Hwang, *Invest. Ophthalmol. Visual Sci.*, 2018, **59**, 1475–1485.
- 18 E. S. Gil, B. B. Mandal, S.-H. Park, J. K. Marchant, F. G. Omenetto and D. L. Kaplan, *Biomaterials*, 2010, **31**, 8953–8963.
- 19 T. Kawakita, K. Higa, S. Shimmura, J. Shimazaki and K. Tsubota, *Invest. Ophthalmol. Visual Sci.*, 2014, **55**, 5156.
- 20 M. Grolik, D. Kuźmicz, D. Dobrowolski, B. Wowra, E. Wylegala, M. Nowakowska and K. Szczubiałka, *J. Biomater. Tissue Eng.*, 2018, **8**, 374–383.
- 21 X. Hu, W. Lui, L. Cui, M. Wang and Y. Cao, *Tissue Eng.*, 2005, **11**, 1710–1717.
- 22 P. Fagerholm, N. S. Lagali, K. Merrett, W. B. Jackson, R. Munger, Y. Liu, J. W. Polarek, M. Söderqvist and M. Griffith, *Sci. Transl. Med.*, 2010, **2**, 46ra61.

- 23 A. I. Van Den Bulcke, B. Bogdanov, N. De Rooze, E. H. Schacht, M. Cornelissen and H. Berghmans, *Biomacromolecules*, 2000, **1**, 31–38.
- 24 J. Rose, S. Pacelli, A. Haj, H. Dua, A. Hopkinson, L. White and F. Rose, *Materials*, 2014, **7**, 3106–3135.
- 25 N. Hasirci, C. Kilic, A. Kömez, G. Bahcecioglu and V. Hasirci, in *Gels Handbook*, ed. M. R. Abidian, U. A. Gurkan and F. Edalat, World Scientific, 2016, vol. 2, pp. 1–52.
- 26 T. Mimura, S. Amano, S. Yokoo, S. Uchida, S. Yamagami, T. Usui, Y. Kimura and Y. Tabata, *Mol. Vision*, 2008, **14**, 1819–1828.
- 27 L. J. Luo, J. Y. Lai, S. F. Chou, Y. J. Hsueh and D. H. K. Ma, *Acta Biomater.*, 2018, **65**, 123–136.
- 28 G. Bahcecioglu, N. Hasirci, B. Bilgen and V. Hasirci, *Biofabrication*, 2019, **11**, 25002.
- 29 G. Bahcecioglu, N. Hasirci, B. Bilgen and V. Hasirci, *Int. J. Biol. Macromol.*, 2019, **122**, 1152–1162.
- 30 G. Eke, N. Mangir, N. Hasirci, S. MacNeil and V. Hasirci, *Biomaterials*, 2017, **129**, 188–198.
- 31 N. Celikkin, S. Mastrogiacomio, J. Jaroszewicz, X. F. Walboomers and W. Swieszkowski, *J. Biomed. Mater. Res., Part A*, 2018, **106**, 201–209.
- 32 L. Li, C. Lu, L. Wang, M. Chen, J. White, X. Hao, K. M. McLean, H. Chen and T. C. Hughes, *ACS Appl. Mater. Interfaces*, 2018, **10**, 13283–13292.
- 33 F. Rengier, A. Mehndiratta, H. von Tengge-Kobligk, C. M. Zechmann, R. Unterhinninghofen, H.-U. Kauczor and F. L. Giesel, *Int. J. Comput. Assist. Radiol. Surg.*, 2010, **5**, 335–341.
- 34 A. Sorkio, L. Koch, L. Koivusalo, A. Deiwick, S. Miettinen, B. Chichkov and H. Skottman, *Biomaterials*, 2018, **171**, 57–71.
- 35 A. Isaacson, S. Swioklo and C. J. Connon, *Exp. Eye Res.*, 2018, **173**, 188–193.
- 36 B. A. Harley, J. H. Leung, E. C. Silva and L. J. Gibson, *Acta Biomater.*, 2007, **3**, 463–474.
- 37 M. Rizwan, G. S. L. Peh, H. P. Ang, N. C. Lwin, K. Adnan, J. S. Mehta, W. S. Tan and E. K. F. Yim, *Biomaterials*, 2017, **120**, 139–154.
- 38 D. Hellio-Serughetti and M. Djabourov, *Langmuir*, 2006, **22**, 8516–8522.
- 39 J. Yin, M. Yan, Y. Wang, J. Fu and H. Suo, *ACS Appl. Mater. Interfaces*, 2018, **10**, 6849–6857.
- 40 Y. S. Zhang, K. Yue, J. Aleman, K. Mollazadeh-Moghaddam, S. M. Bakht, J. Yang, W. Jia, V. Dell'Erba, P. Assawes, S. R. Shin, M. R. Dokmeci, R. Oklu and A. Khademhosseini, *Ann. Biomed. Eng.*, 2017, **45**, 148–163.
- 41 B. Jeong, S. W. Kim and Y. H. Bae, *Adv. Drug Delivery Rev.*, 2012, **64**, 154–162.
- 42 Q. Chen, L. Zhu, C. Zhao, Q. Wang and J. Zheng, *Adv. Mater.*, 2013, **25**, 4171–4176.
- 43 H. B. Bohidar and S. S. Jena, *J. Chem. Phys.*, 1993, **98**, 8970–8977.
- 44 L. E. Bertassoni, J. C. Cardoso, V. Manoharan, A. L. Cristino, N. S. Bhise, W. A. Araujo, P. Zorlutuna, N. E. Vrana, A. M. Ghaemmaghami, M. R. Dokmeci and A. Khademhosseini, *Biofabrication*, 2014, **6**, 024105.
- 45 D. Joung, V. Truong, C. C. Neitzke, S.-Z. Guo, P. J. Walsh, J. R. Monat, F. Meng, S. H. Park, J. R. Dutton, A. M. Parr and M. C. McAlpine, *Adv. Funct. Mater.*, 2018, 1801850.
- 46 C. Colosi, S. R. Shin, V. Manoharan, S. Massa, M. Costantini, A. Barbetta, M. R. Dokmeci, M. Dentini and A. Khademhosseini, *Adv. Mater.*, 2015, **28**, 677–684.
- 47 B. Hoffmann and C. Schäfer, *Cell Adhes. Migr.*, 2010, **4**, 190–193.
- 48 D. B. Kolesky, R. L. Truby, A. S. Gladman, T. A. Busbee, K. A. Homan and J. A. Lewis, *Adv. Mater.*, 2014, **26**, 3124–3130.
- 49 R. M. Gouveia, E. Koudouna, J. Jester, F. Figueiredo and C. J. Connon, *Adv. Biosyst.*, 2017, **1**, 1700135.
- 50 J. L. Battaglioli and R. D. Kamm, *Invest. Ophthalmol. Visual Sci.*, 1984, **25**, 59–65.
- 51 S. J. Petsche, D. Chernyak, J. Martiz, M. E. Levenston and P. M. Pinsky, *Invest. Ophthalmol. Visual Sci.*, 2012, **53**, 873–880.
- 52 P. Zorlutuna, N. Builles, O. Damour, A. Elsheikh and V. Hasirci, *Biomaterials*, 2007, **28**, 3489–3496.
- 53 N. E. Vrana, A. Elsheikh, N. Builles, O. Damour and V. Hasirci, *Biomaterials*, 2007, **28**, 4303–4310.
- 54 C. Kilic Bektas and V. Hasirci, *J. Mater. Sci. Mater. Med.*, 2019, (recently accepted for publication).
- 55 T. S. Girton, T. R. Oegema, E. D. Grassl, B. C. Isenberg and R. T. Tranquillo, *J. Biomech. Eng.*, 2000, **122**, 216–223.
- 56 T. S. Girton, T. R. Oegema and R. T. Tranquillo, *J. Biomed. Mater. Res.*, 1999, **46**, 87–92.
- 57 M. A. Watsky, C. J. Doillon, M. Hakim, J. Wang, R. Munger, N. Laycock and M. Griffith, *Invest. Ophthalmol. Visual Sci.*, 2002, **43**, 2996.
- 58 S. R. Sloan, M. A. R. Garcia, Y. Khalifa and M. R. Buckley, *Invest. Ophthalmol. Visual Sci.*, 2015, **56**, 1108.
- 59 J. V. Jester, P. A. Barry-Lane, H. D. Cavanagh and W. M. Petroll, *Cornea*, 1996, **15**, 505–516.
- 60 G. P. Riley, R. L. Harrall, P. G. Watson, T. E. Cawston and B. L. Hazleman, *Eye*, 1995, **9**(Pt 6), 703–718.
- 61 J. M. Sivak and M. E. Fini, *Prog. Retinal Eye Res.*, 2002, **21**, 1–14.
- 62 J. D. Mallet and P. J. Rochette, *Photochem. Photobiol. Sci.*, 2013, **12**, 1310–1318.
- 63 C. Kilic Bektas, A. Burcu, G. Gedikoglu, H. H. Telek, F. Ornek and V. Hasirci, *J. Biomater. Sci., Polym. Ed.*, 2019, **30**, 1803–1821.